Supporting Information

Ershov et al. 10.1073/pnas.1222196110

SI Text

Synthesis of Core-Shell Particles. Core-shell particles consisting of a fluorescent polystyrene core and a shell of poly(*N*-isopropyl acrylamide-comethacrylic acid) were synthesized adopting a protocol described previously (1) in a two-step procedure. *N*-isopropylacrylamide (NIPAm), N,N′-methylenebisacrylamide (BIS), methacrylic acid (MAc), potassium peroxodisulfate (KPS), styrene, and SDS were purchased from Sigma-Aldrich. The fluorescent dye pyrromethene 546 was purchased from Exciton.

First, fluorescent cores, with a diameter $d \simeq 300$ nm, and polydispersity <5% were prepared in an emulsion polymerization; 7.9 g of styrene, 0.75 g of NIPAm, 25 mg of SDS, and 5 mg of fluorescent label were mixed with 26 mL of deionized (DI) water. Following 15 min of purging the reaction mixture with N_2 at 80 °C to remove dissolved oxygen, the reaction was initiated with 20 mg of KPS, dissolved in 1 mL water. The reaction was left for 40 h at 80 °C. The cores were purified by repeated centrifugation and resuspension in water.

A nonfluorescent microgel shell was grown around the core through precipitation copolymerization of NIPAm and MAc with the cross-linker BIS, approximately 1-g cores in 100 mL of water, 2.7 g of NIPAm, 58 mg of BIS, and 210 μL of MAc. After 15 min of purging with N_2 at 80 °C, the reaction was initiated with 100 mg of KPS dissolved in 5 mL water. The reaction was allowed to proceed for 2 h at 80 °C.

The core-shell particles were purified by repeated centrifugation and resuspension in 1 mM NaOH in DI water and concentrated to ∼10 wt%, stored as a concentrated stock suspension at 4 °C. Before using in experiments core-shell particles were washed and resuspended in DI water. The final size of the core-shell particles was determined by dynamic light scattering and is 1.2 μm.

Analysis of Interface Curvature. Particles adsorbed at the curved liquid interfaces were imaged with a Zeiss Axiovert 200M-Exciter confocal laser scanning microscope. Three-dimensional z-stacks were taken, with a pinhole of 60 μm, corresponding to a slice thickness of 0.4 μm. The resulting image sequence was analyzed using a MATLAB (MathWorks) script for 3D particle tracking from the Kilfoil laboratory (2), with a resolution of ∼20 nm in plane and 50 nm in the z-direction. From this, three-dimensional particle coordinates were extracted. Particles not adsorbed to the interface were excluded from the analysis.

The time-averaged particle coordinates were interpolated to obtain a smooth description of the liquid interface, using a MATLAB script written by John D'Errico (3). We describe the interface in the Monge representation (3) as $F(x,y,z) = z - h(x,y) = 0$, where $h(x,y)$ is the local height above the xy plane at coordinates (x,y), as obtained from the interpolation script. We then find the local shape operator of the interface at each location as (4)

$$Q_{ij} = \frac{1}{\Upsilon}\left[F_{ij} - \frac{F_i \Upsilon_j}{\Upsilon}\right],$$

where $\Upsilon = |\nabla F| = (1+h_x^2+h_y^2)^{1/2}$ and where $F_i = \partial F/\partial r_i$ and $\Upsilon_i = \partial \Upsilon/\partial r_i$ with $\mathbf{r} = (x,y,z)$. The shape operator $\mathbf{Q}$ is a tensor, describing how the normal vector on the interface varies spatially. The two eigenvalues of $\mathbf{Q}$ with the dimension of an inverse length are the principal curvature values κ_1 and κ_2 and the corresponding eigenvectors are the principal directions (3). The tensor $\mathbf{Q}$ has two nonzero invariants (scalars that do not depend on the choice of the coordinate system), which can both be written in terms of the eigenvalues. The first is the mean curvature, $H = \frac{1}{2}(\kappa_1 + \kappa_2)$, which is equal to half the trace of $\mathbf{Q}$. The other invariant (the sum of the principal minors) is called the Gaussian curvature and is equal to the product of the two eigenvalues, $K = \kappa_1\kappa_2$. The deviatoric curvature, $D = \frac{1}{2}|\kappa_1 - \kappa_2|$ can be written as a combination of the two invariants H and K: $D = \sqrt{H^2 - K}$. It is clear, therefore, that D is also an invariant of the curvature tensor (i.e., it does not depend on the coordinate system that is chosen) (5).

Fig. S2 shows an example of our analysis of the interface curvature for a region on an anisotropically curved droplet. The principal curvature directions at each particle position are shown as black lines and the color scale indicates the value of the deviatoric curvature. It can be seen how particles are dispersed in the area where $D < 0.002\ \mu\text{m}^{-1}$, whereas above this threshold they organize in a square lattice aligned along the principal directions.

Selection of Nearest Neighbors and Determination of Order Parameter. For the analysis of the particle organization, it is necessary to first choose the neighbors of each particle. For cases in which the particle distribution is homogeneous, this can be done by selecting only those particles as neighbors that are at a distance that falls within a certain range around the first peak of the radial distribution function (Fig. S3*A*). However, this approach fails in our systems because the interparticle distance depends on the deviatoric curvature and becomes shorter when the interface is curved stronger, due to stronger attraction. Hence, the neighbor selection criterion should depend on position. We therefore choose neighbors individually for each particle. First, the nearest particle is found for each particle; if that particle is at a distance L, then all particles within a distance $1.3L$ are considered as neighbors. This excludes the particles at an angle of 45° in the square lattice, which are at a distance $\sqrt{2}L$. To show that this method works we indicate the number of neighbors with a color code in Fig. S3*B*.

Once the neighbors for each particle are selected, we calculate for each pair of neighboring particles the angle φ between the bond between them and the local direction of principal curvature, and we construct a probability histogram of φ. An example is given in Fig. 2*B*, and more examples are given below in Figs. S4–S6. As a measure for the local order we choose the order parameter $\cos(4\varphi)$; values of this order parameter for various interfaces are also shown in Figs. S4–S6. For ideal alignment, φ is either 0° or 90°, so that $\cos(4\varphi) = 1$, whereas for a completely random distribution $\cos(4\varphi) = 0$. As shown in Fig. 2*C*, $\cos(4\varphi)$ reaches a value of ∼0.6 at high deviatoric curvatures. Defects in the lattice preclude higher values, although in small regions with few defects $\cos(4\varphi)$ can become as high as 0.8 (Fig. S5*F*).

Note that for very low particle densities, such as for the interfaces in Figs. S4*A* and S5*A*, it is not possible to reliably determine the principal axes. Constructing the probability distribution of angles φ is difficult in this case. We therefore analyze these movies differently: We track the particles for several minutes, and for each frame we calculate the distance r between each pair of particles. We then construct a probability histogram $P(r)$ of particle separations. As shown in Fig. S5*B*, $P(r)$ has a sharp peak at the typical particle–particle separation for curved interfaces, where the particles attract each other. By contrast, on a flat interface (Fig. S4*B*) the particles avoid each other, giving a broad peak at much larger distance, which is due to repulsion between the particles.

1. Perro A, Meng G, Fung J, Manoharan VN (2009) Design and synthesis of model transparent aqueous colloids with optimal scattering properties. *Langmuir* 25(19): 11295–11298.
2. Kilfoil M. Kilfoil laboratory scripts for particle tracking. Available at http://people.umass.edu/kilfoil/downloads.html. Accessed May, 2012.
3. D'Errico J (2005) Script for interface interpolation. Available at www.mathworks.com/matlabcentral/fileexchange/8998-surface-fitting-using-gridfit. Accessed May, 2012.
4. Safran SA (1994) *Statistical Thermodynamics of Surfaces, Interfaces, and Membranes* (Addison-Wesley, Reading, MA).
5. Iglic A, Kralj-Iglic V (2003) Effect of anisotropic properties of membrane constituents on stable shapes of membrane bilayer structure. *Planar Lipid Bilayers (BLMs) and Their Applications*, eds Tien HT, Ottova-Leitmannova A (Elsevier, Amsterdam).

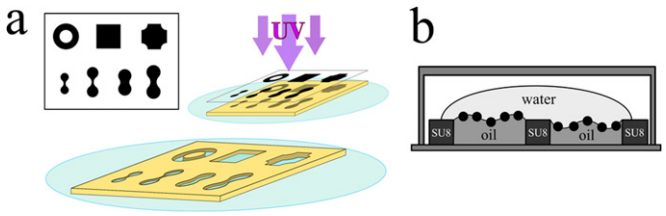

Fig. S1. Preparation of patterned slides. (*A*) A layer of SU-8 photoresist is spin-coated on a glass slide and then UV-cross-linked through a photomask. After washing away the noncross-linked photoresist with propylene glycol methyl ether acetate, a 25-μm-thick layer of SU-8 with wells in it is formed. (*B*) Oil droplets are deposited in the wells and covered with a layer of water; added particles bind to the oil/water interface. The sample was sealed in a glass chamber to prevent evaporation.

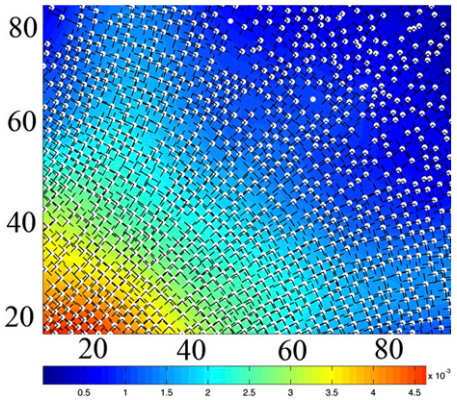

Fig. S2. Deviatoric curvature and principal directions on an anisotropic interface. Interpolation of particle positions gives a smooth description of the interface. From this, principal curvature values and directions are obtained. Deviatoric curvature is indicated with color (numbers below colorbar indicate D in micrometers^{-1}). The black lines indicate the directions of local principal curvatures at each particle center. Axes of the figure give relative position in micrometers.

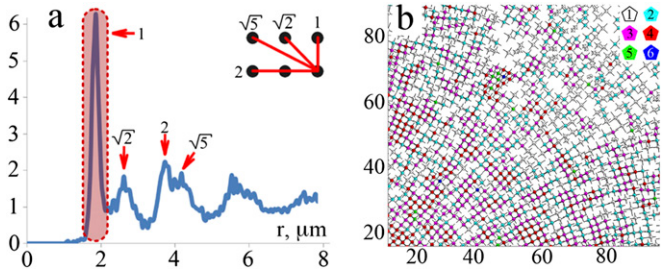

Fig. S3. Neighbor selection. Selecting neighbors based on the peak in the radial distribution function (*A*) fails, because the interparticle distance depends on deviatoric curvature. Therefore, a local selection criterion is used (*SI Text*). (*B*) Distribution of number of neighbors. Color indicates number of neighbors: white, 1; cyan, 2; magenta, 3; red, 4; green, 5; and blue, 6. Axes of the figure give relative position in micrometers.

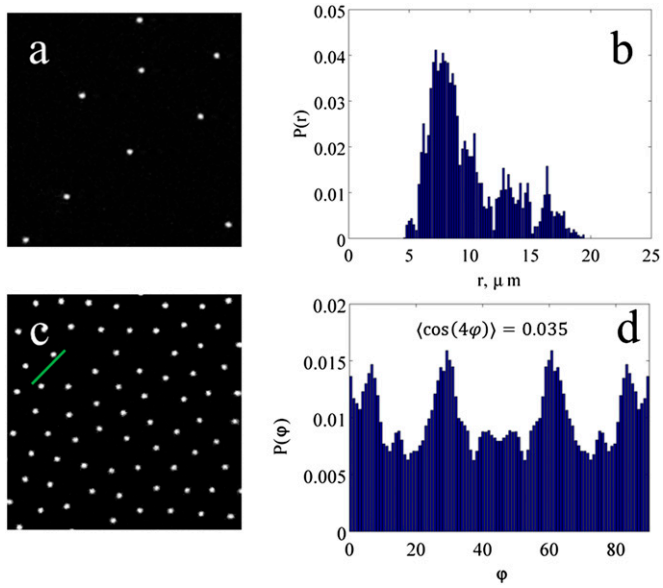

Fig. S4. Particles at a flat interface do not attract each other. (*A*) Snapshot of particles adsorbed at a flat interface at a density of 0.03 μm^{-2} (from Movie S1). (*B*) Probability distribution $P(r)$ of separations r between particles obtained from Movie S1. The peak is at 8 μm, much larger than the particle diameter (1.2 μm), and interparticle separations smaller than 5 μm are very unlikely. This indicates a long-ranged repulsion between the particles. (*C*) Snapshot of particles adsorbed at a flat interface at a density of 0.26 μm^{-2} (from Movie S2). The average distance between neighboring particles is ∼1.9 μm in this figure. (*D*) Probability distribution $P(\phi)$ of angles between interparticle bonds and an arbitrarily chosen axis, indicated by the green line in *C*. The distribution has peaks separated by 30° and the order parameter $\cos(4\phi) \approx 0.035$ for this interface, whereas $|\psi_6| \approx 0.66$ (indicating hexagonal order).

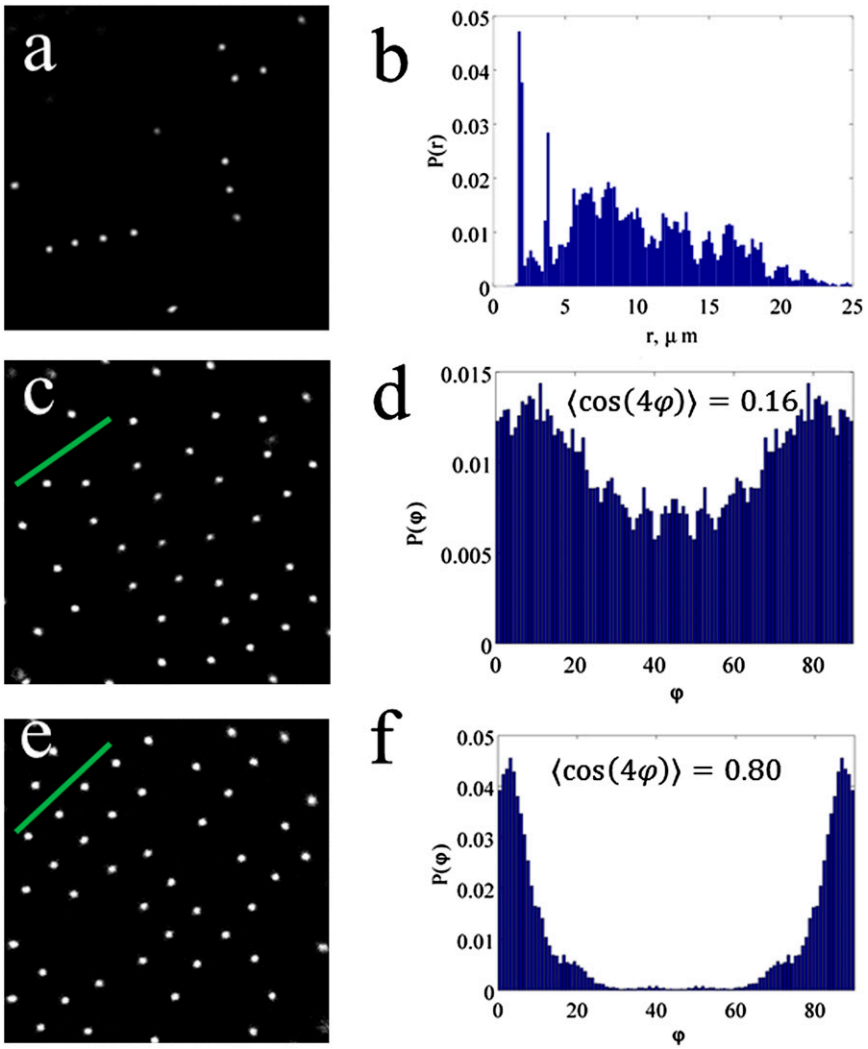

Fig. S5. Particles at anisotropically curved interfaces attract by quadrupolar interactions. (*A*) Snapshot of particles adsorbed at a density of 0.03 μm^{-2} at the interface of a dumbbell-shaped droplet ($D > 0.003\ \mu m^{-1}$) showing the formation of linear particle arrays (from Movie S3). (*B*) Probability distribution $P(r)$ of particle separations r obtained from Movie S3. $P(r)$ has a peak at a distance of 2 μm and a second peak at twice this distance, indicating an attractive interaction between the particles. (*C*) Snapshot of particles at a curved interface with $D \sim 0.002\ \mu m^{-1}$ at a density of 0.2 μm^{-2} (from Movie S4); (*D*) probability distribution $P(\phi)$ of angles between interparticle bonds and the principal curvature axis indicated by the green line in *C*. The value of D is close to the onset of ordering. (*E*) Snapshot of particles at a curved interface with $D \sim 0.004\ \mu m^{-1}$ at a density of 0.2 μm^{-2} (from Movie S5); (*F*) probability distribution $P(\phi)$ of angles between interparticle bonds and the principal curvature axis indicated by the green line in *E*. Average values of $\cos(4\phi)$ are indicated above the histograms in *D* and *F*; furthermore $|\psi_4| \approx 0.59$ in *D* and $|\psi_4| \approx 0.92$ in *F*.

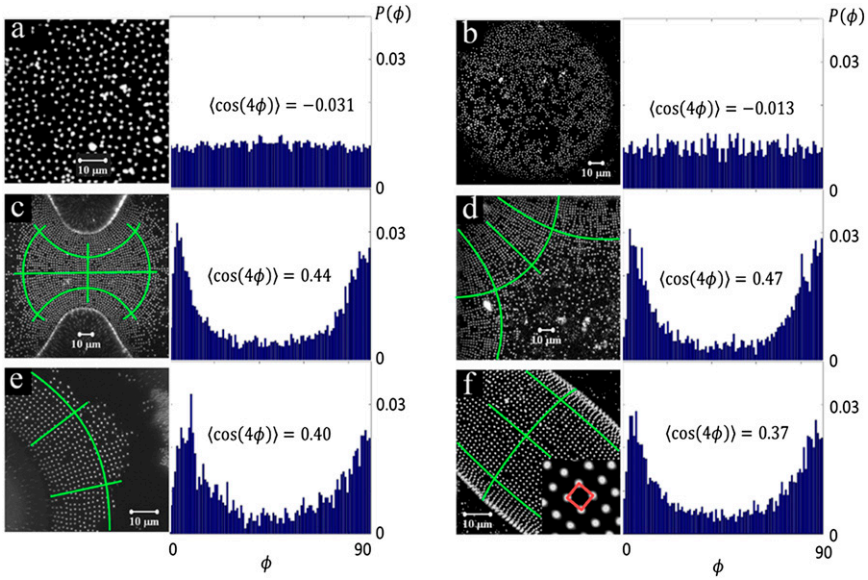

Fig. S6. Analysis of particle organizations in Fig. 1. Probability distributions of angles ϕ between interparticle bonds and the local principal curvature axes for the interfaces of Fig. 1. (*A*) A flat interface, (*B*) a spherical interface, (*C*) a dumbbell-shaped droplet, (*D*) a droplet pinned to a square patch (only one corner is shown), (*E*) a toroid-shaped droplet, and (*F*) a prolate ellipsoid. The average value of the order parameter, $\cos(4\varphi)$, is indicated for each case. Principal axes in *C*–*F* are indicated with green lines; in *A* and *B* the horizontal axis is chosen as reference axis. The bond orientational order parameters for these images are *A*, $|\psi_4| \approx 0.47$, $|\psi_6| \approx 0.49$; *B*, $|\psi_4| \approx 0.46$, $|\psi_6| \approx 0.52$; *C*, $|\psi_4| \approx 0.71$, $|\psi_6| \approx 0.36$; *D*, $|\psi_4| \approx 0.83$, $|\psi_6| \approx 0.18$; *E*, $|\psi_4| \approx 0.73$, $|\psi_6| \approx 0.36$; and *F* $|\psi_4| \approx 0.76$, $|\psi_6| \approx 0.27$. (Scale bar, 10 μm in all images.)

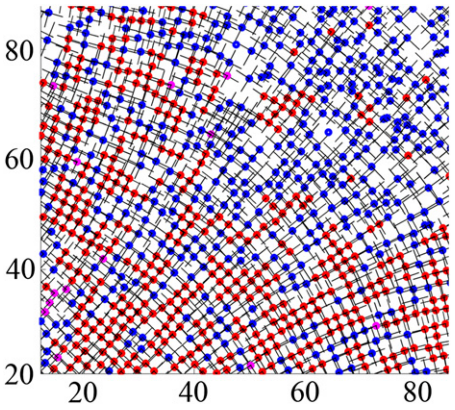

Fig. S7. Local order parameter on an anisotropically curved interface. The average order parameter $\cos(4\varphi)$ is calculated for each particle and indicated with a color code. Blue, $\cos(4\varphi) < 0.3$; magenta, $0.3 < \cos(4\varphi) < 0.4$; red, $\cos(4\varphi) > 0.4$. Axes of the figure give relative position in micrometers.

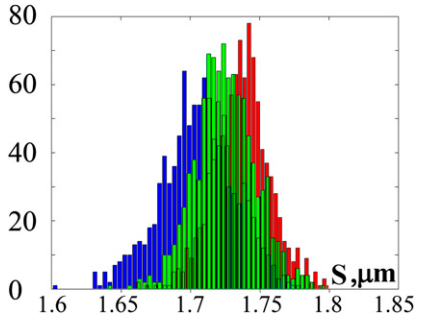

Fig. S8. Probability distribution of particle separations *S*. Time-lapse movies of particles at curved interfaces (Movies S3, S4, S5, and S6) were analyzed by tracking the particles and making histograms of separations between neighboring particles. Three examples for three different particle pairs are shown. Histograms for particles corresponding to the same average interparticle separation and same deviatoric curvature were added and used to obtain the effective pair interaction potential shown in Fig. 2*D*.

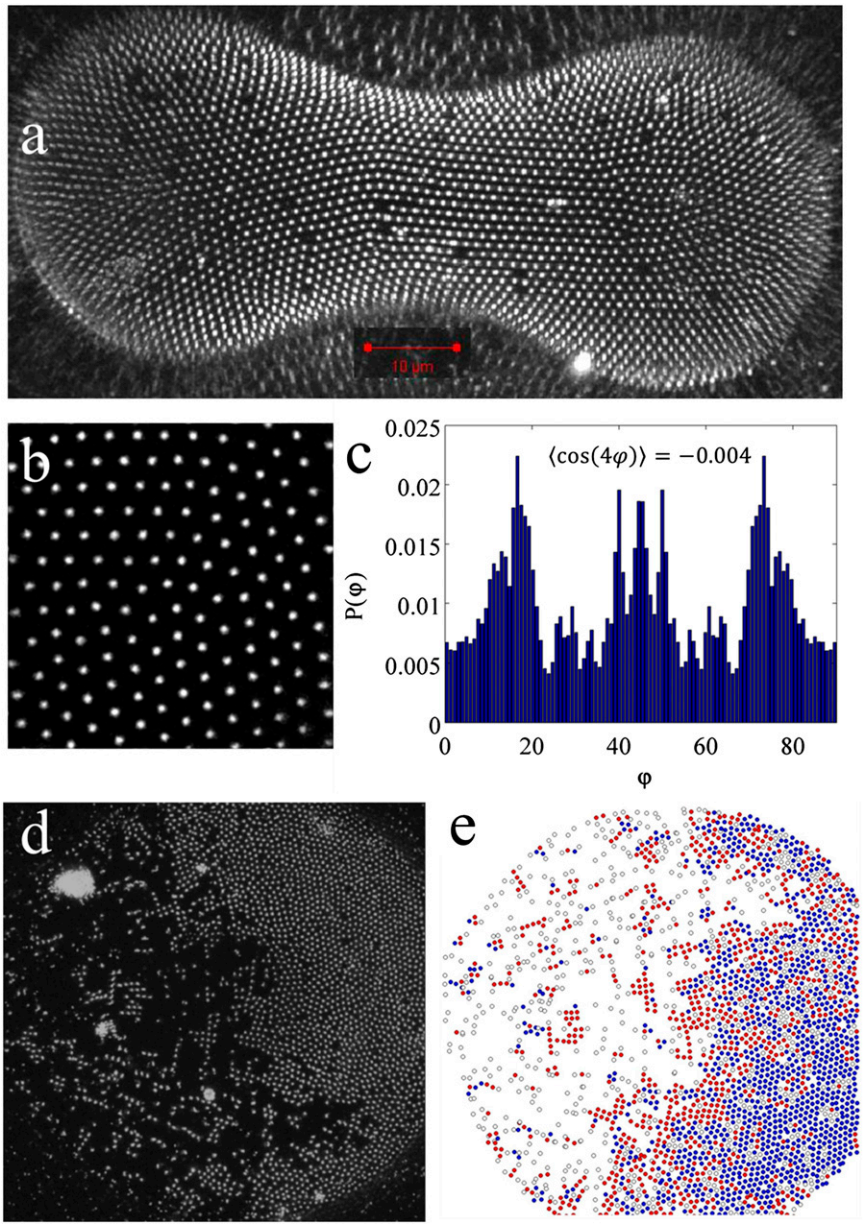

Fig. S9. At high particle density the organization is hexagonal. (*A*) A dumbbell-shaped droplet covered with colloidal particles at high density. The particles are organized in a hexagonal lattice ($|\psi_6| = 0.74$). (*B*) Snapshot of particles adsorbed at a dumbbell-shaped interface at high density, ~0.5 μm^{-2} (from Movie S7); (*C*) probability distribution $P(\phi)$ of angles between interparticle bonds and the horizontal direction, showing peaks separated by 30°. Note that the presence of a grain boundary in this sample leads to multiple sets of peaks in the angle distribution. For this example, $\cos(4\phi) \approx -0.004$, whereas $|\psi_4| \approx 0.11$ and $|\psi_6| \approx 0.73$, indicating hexagonal order. (*D*) Part of a dumbbell-shaped droplet, partially covered with particles. There is a coexistence between square and hexagonal organization. (*E*) Color-coded picture of *D*: Particles in square ordering ($|\psi_4| > |\psi_6|$) are shown in red; particles in hexagonal organization ($|\psi_4| < |\psi_6|$) are shown in blue.

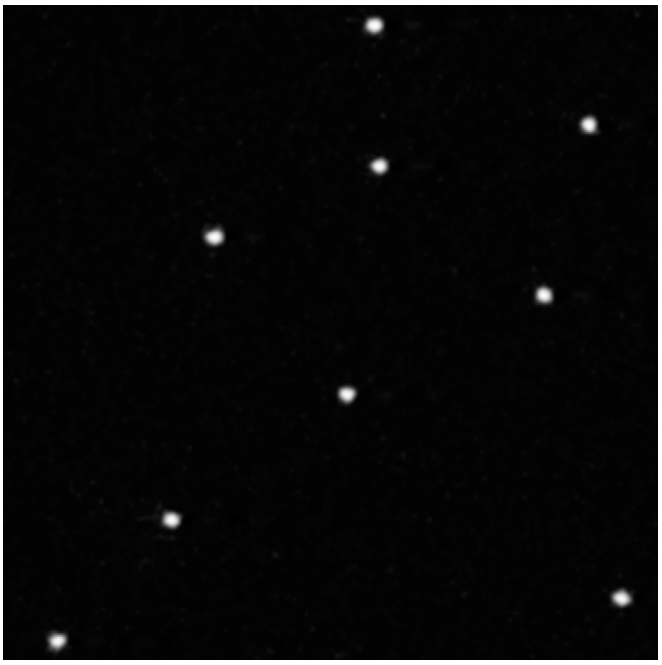

Movie S1. Particles at a flat interface (low density). Particles adsorbed at a flat interface ($D \approx 0$) at low density ($\sim$0.03 μm^{-2}). The particles move around without coming into close proximity. A probability histogram of the distance between particles for this movie is shown in Fig. S4*B*; it shows that particles do not come closer than $\sim$5 μm, and indicates long-ranged repulsion between the particles.

Movie S1

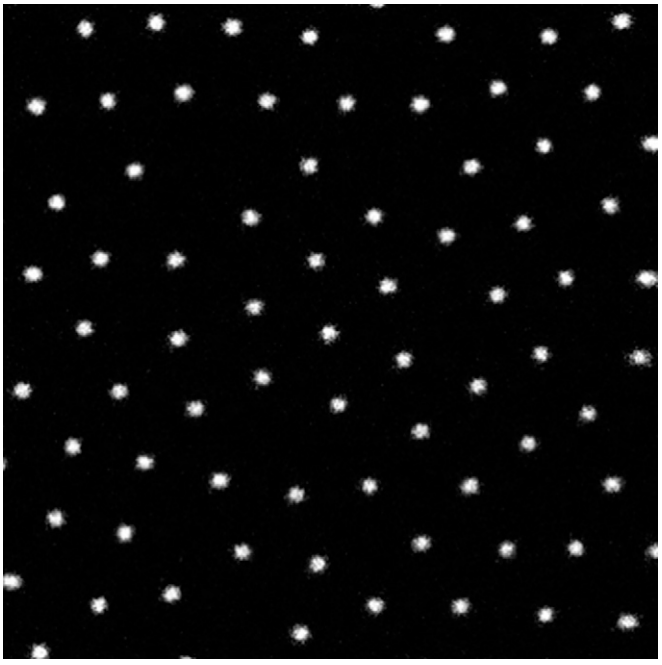

Movie S2. Particles at a flat interface (higher density). Particles adsorbed at a flat interface ($D \approx 0$) at higher density ($\sim$0.3 μm^{-2}, average separation distance between particles is 1.9 μm). The particles no longer move freely at this density, owing to (isotropic) repulsion between the particles. Packing constraints lead to a hexagonal organization (see also Fig. S4*B*).

Movie S2

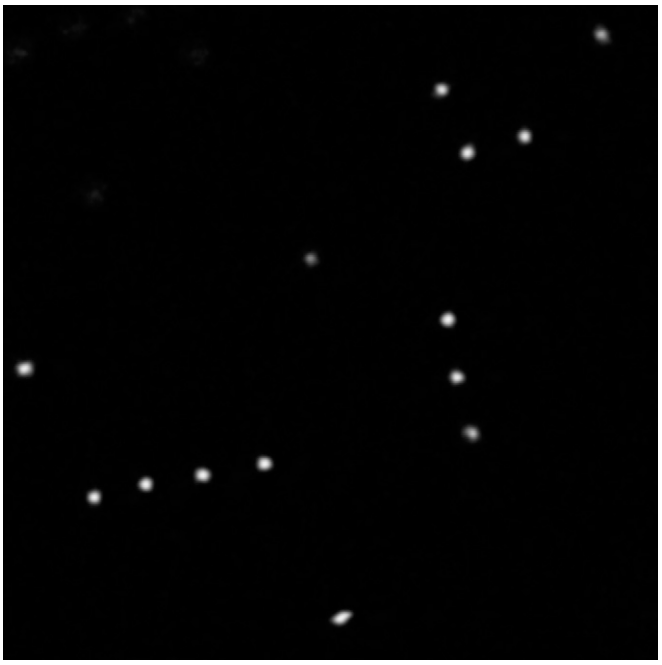

Movie S3. Particles at an anisotropically curved interface (low density). Particles adsorbed at a curved interface ($D > 0$) at low density ($\sim$0.03 μm^{-2}). The particles arrange in linear arrays along two perpendicular directions, indicating a quadrupolar attraction between the particles. A probability histogram of the distance between particles for this movie is shown in Fig. S5*B*.

Movie S3

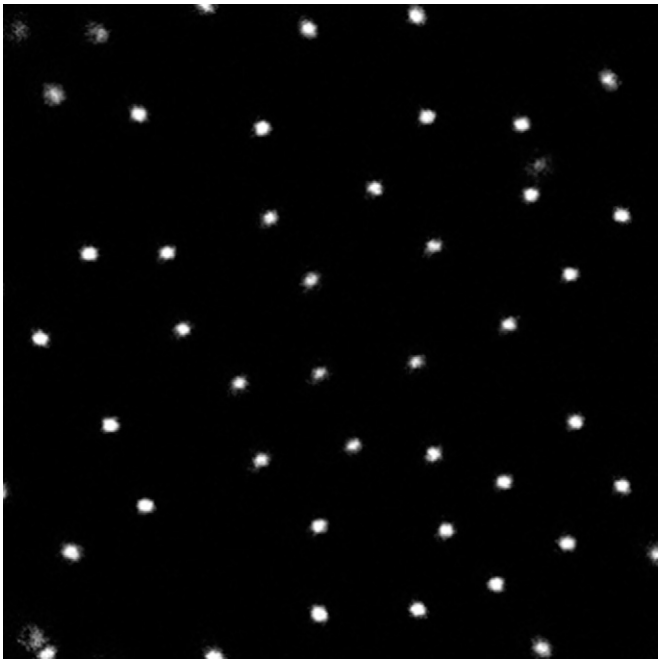

Movie S4. Particles at a weakly anisotropically curved interface. Particles adsorbed at an interface with small but finite deviatoric curvature ($D \approx 0.002$ μm^{-1}) at a density of $\sim$0.2 μm^{-2}. Particles transiently organize in local square arrangements. At this small value of D, the square lattice is not very stable, and there is still a lot of mobility. A histogram of the angles between interparticle bonds and the principal curvature axis for this movie is shown in Fig. S5*D*.

Movie S4

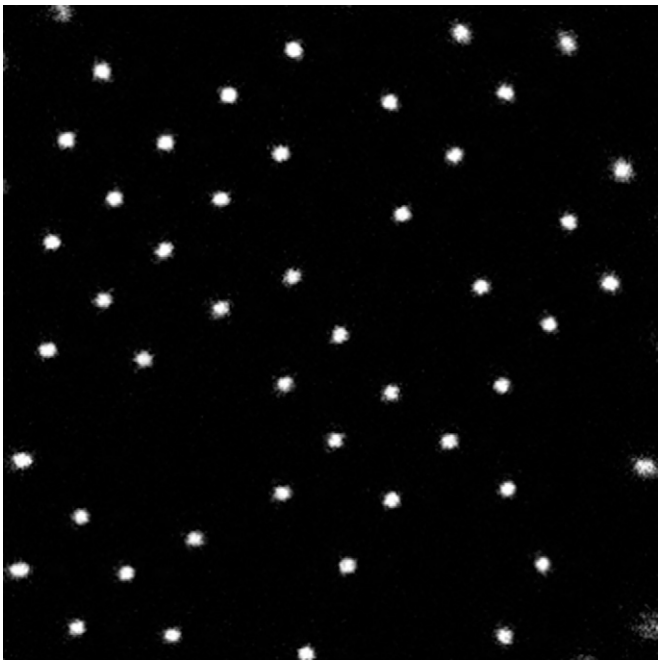

Movie S5. Particles at an anisotropically curved interface. Particles adsorbed at an interface with a deviatoric curvature $D \approx 0.004\ \mu m^{-1}$ at a density of $\sim 0.2\ \mu m^{-2}$. Particles organize in local square arrangements that persist during the duration of the movie. A histogram of the angles between interparticle bonds and the principal curvature axis for this movie is shown in Fig. S5*F*.

Movie S5

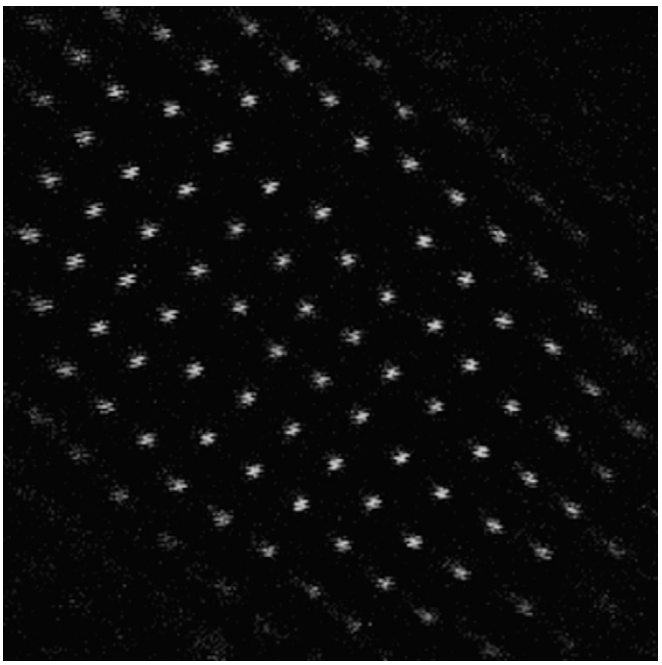

Movie S6. Particles at an ellipsoidal droplet. Particles adsorbed at an ellipsoidal droplet at a density of $\sim 0.2\ \mu m^{-2}$. Particles organize in a square lattice and vibrate around their average lattice position.

Movie S6

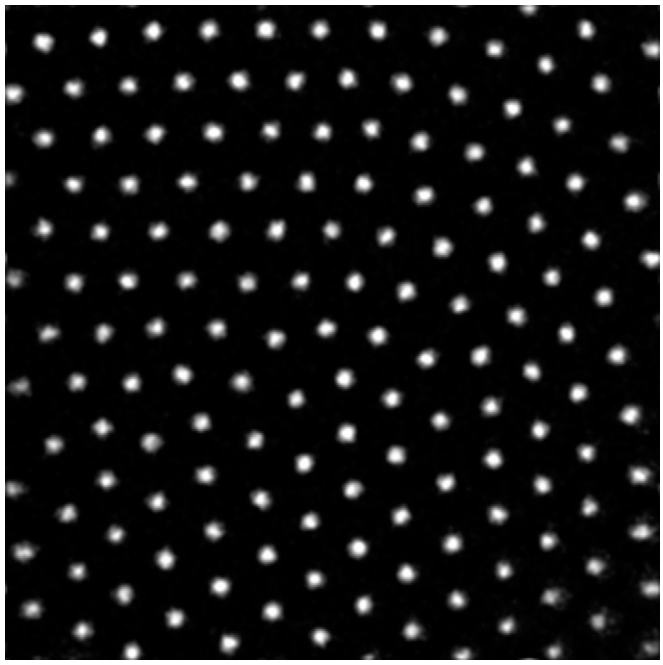

Movie S7. Particles at an anisotropically curved interface at high density. Particles adsorbed at an interface with a deviatoric curvature $D \approx 0.002\ \mu m^{-1}$ at a density of $\sim 0.5\ \mu m^{-2}$. At this high density, packing constraints force the particles in a hexagonal lattice (see also Fig. S9*C*).

Movie S7